


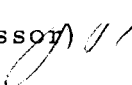
AN ABSTRACT OF THE THESIS OF

Philip Royal Laun for the M. S. in Oceanography
(Name) (Degree) (Major)

Date thesis is presented 9 December 1964

Title PRIMARY SEISMIC WAVE (P) AT 250-350 KM COMPARED
TO MEASURED WAVE AT 0.3 KM FROM GNOME NUCLEAR
EXPLOSION

Redacted for Privacy

Abstract approved _____
 (Major professor) 

The first cycle of seismic waves recorded at distances of 245, 300 and 355 km. from the GNOME nuclear explosion was used to determine whether the near source wave characteristics at 0.3 km. could be determined from distance measurements. Both head wave and body wave propagation were considered. First the recorded signals at distance were inversely propagated back to the near source region as head waves, and secondly, the measured source at 0.3 km. was propagated out to 300 km. from the source as a body wave. In both cases, restricted comparisons between theory and observation can be made, but the comparison appears to favor the body wave type of propagation. More research is needed to make a more conclusive choice between the two modes of propagation. Methods were developed which can be used to determine source motion from distance measurements when the data are sufficient to do so.

PRIMARY SEISMIC WAVE (P) AT 250-350 KM
COMPARED TO MEASURED WAVE AT 0.3 KM
FROM GNOME NUCLEAR EXPLOSION

by

PHILIP ROYAL LAUN

A THESIS

submitted to

OREGON STATE UNIVERSITY

in partial fulfillment of
the requirements for the
degree of

MASTER OF SCIENCE

June 1965

APPROVED:

Redacted for Privacy

Professor of Oceanography *J. S.*
In Charge of Major

Redacted for Privacy

Head of Department of Oceanography

Redacted for Privacy

Dean of Graduate School

Date thesis is presented *9 December 1964*

Typed by Marion F. Palmateer

ACKNOWLEDGEMENTS

The writer is indebted to Dr. Joseph W. Berg Jr. for guidance in all phases of the research and manuscript.

The writer thanks his wife, Judith Anne, for her help in preparing the manuscript and Mr. Stanley H. Borders for critical readings and comments.

This research was supported by the Air Force Office of Scientific Research under Grant AF-AFOSR-49(638)-1403 as part of the VELA UNIFORM Program directed by the Advanced Research Projects Agency of the Department of Defense.

TABLE OF CONTENTS

	<u>Page</u>
INTRODUCTION	1
DATA	3
ANALYSIS OF THE DATA	14
DISCUSSION OF RESULTS	33
SUMMARY	40
BIBLIOGRAPHY	42
APPENDICES	
APPENDIX I	45
APPENDIX II	48
APPENDIX III	51
APPENDIX IV	54

LIST OF FIGURES

<u>Figure</u>		<u>Page</u>
1	Index Map Showing Seismic Recording Locations for the GNOME Explosion	4
2	Tracings of Records of Ground Motion Used in this Research and Hodographs Showing Character of Ground Motion	6
3	Frequency Spectrum of Vertical Component of Trace Motion as Recorded at Station KILO	10
4	Theoretical Instrument Response Characteristics for Hall-Sears (HS-10) Seismometers	11
5	Response Characteristics of Amplification and Recording System	12
6	Derived Confined Motion of Ground in Microns/sec for Frequencies 3-10 cps Using The First Cycle of Trace Motion	19
7	Graphs of Velocity Potential, Particle Velocity, and Frequency Spectrum, Case I.	24
8	Graphs of Velocity Potential and Particle Velocity, Case II.	25
9	Filtered Calculated Source Potentials for $Q = 250$	30
10	Filtered Calculated Source Potentials for $Q = 500$	31
11	Filtered Calculated Source Potentials for $Q = 800$	32
12	Body Velocity at 300 km. from Source Potential, Case II	36

LIST OF TABLES

<u>Table</u>		<u>Page</u>
I	Source Information of the GNOME Nuclear Explosion	3
II	Calibration of Amplifier and Recording Oscillograph for Frequencies from 1 to 30 cps.	8
III	Crustal Model	15
IV	Amplitude Ratios of Vertical and Horizontal Surface Motion to Incident Compressional Motion for Different Angles of Emergence	17
V	Amplitude Ratio of Transmitted Compressional Wave to Incident Compressional Wave for Crustal Model Layers	20
VI	Averaged First Peak Amplitudes for the Calculated Source Potentials for INDIA, HOTEL and KILO Compared with First Peak Amplitudes for Case I and Case II Potentials	34

PRIMARY SEISMIC WAVE (P) AT 250-350 KM
COMPARED TO MEASURED WAVE AT 0.3 KM
FROM GNOME NUCLEAR EXPLOSION

INTRODUCTION

The purpose of this research was to determine the near source amplitudes of the primary seismic waves generated by the GNOME nuclear explosion using the first compressional seismic wave arrivals recorded at distances of 245, 300 and 355 km. from the explosion. In essence, the problem involved:

- a) Determination of ground motion from records of seismographs located at distances of 245, 300 and 355 km. from the GNOME explosion;
- b) Inverse propagation of this ground motion back to the near source region through an empirically determined or assumed geological model;
- c) Computation of wave form and amplitude of the primary seismic waves that were reduced to the near source region;
- d) Comparison of the results with similar data derived from recordings of ground motion from instruments located within a few kilometers of the source.

For the distances involved in this research, 245 to 355 km., the compressional seismic wave that travels along the base of the earth's crust (Mohorovicic, M, discontinuity) should be the first wave recorded (16, p. 1024). Werth and Herbst (21) and Werth, Herbst and Springer (20) generated waves from a derived source function to simulate the refracted waves from the M discontinuity arriving at

distances between 250 to 700 km. from the source. These waves were compared to the recorded waves at similar distances. In order to compare favorably, additional source energy in the form of a large (three times the normal) free surface reflection had to be assumed.

The problem of determining near source field characteristics (wave form and amplitudes) using seismic pulses recorded at great distances from the source is very difficult. Many approximations had to be made about the transmission of the energy through the earth. For this research, the geological model, through which the energy was theoretically propagated, was empirically determined. The wave propagation paths were chosen to be consistent with theoretical predictions for the given geological model. Attenuation constants were chosen consistent with data reported by other investigators. Thus, using data from a well documented seismic source, such as the GNOME explosion, some of the theories regarding seismic wave propagation were tested. It was the ultimate purpose of this research to provide a more complete understanding of the transmission of seismic waves through the earth.

DATA

Table I gives pertinent information about the GNOME nuclear explosion which was the seismic source for data used in this research.

Table I. Source Information of the GNOME Nuclear Explosion

Name	GNOME
Date	December 10, 1961
Time of detonation*	12:00:00.0 MST
Yield**	3 kt
Latitude*	32° 15' 49" N
Longitude*	103° 51' 57" W

* (16, p. 1017)

** (19, p. 981)

Seismic waves from this source were recorded by the U. S. Geological Survey at stations INDIA, HOTEL and KILO located at 245, 300 and 355 km., respectively, from the source. Figure 1 is an index map showing the locations of the explosion and the three recording stations from which data were obtained for this research. Other stations recorded seismic waves from the blast, but these three stations were chosen because of quantity of data and region of interest.

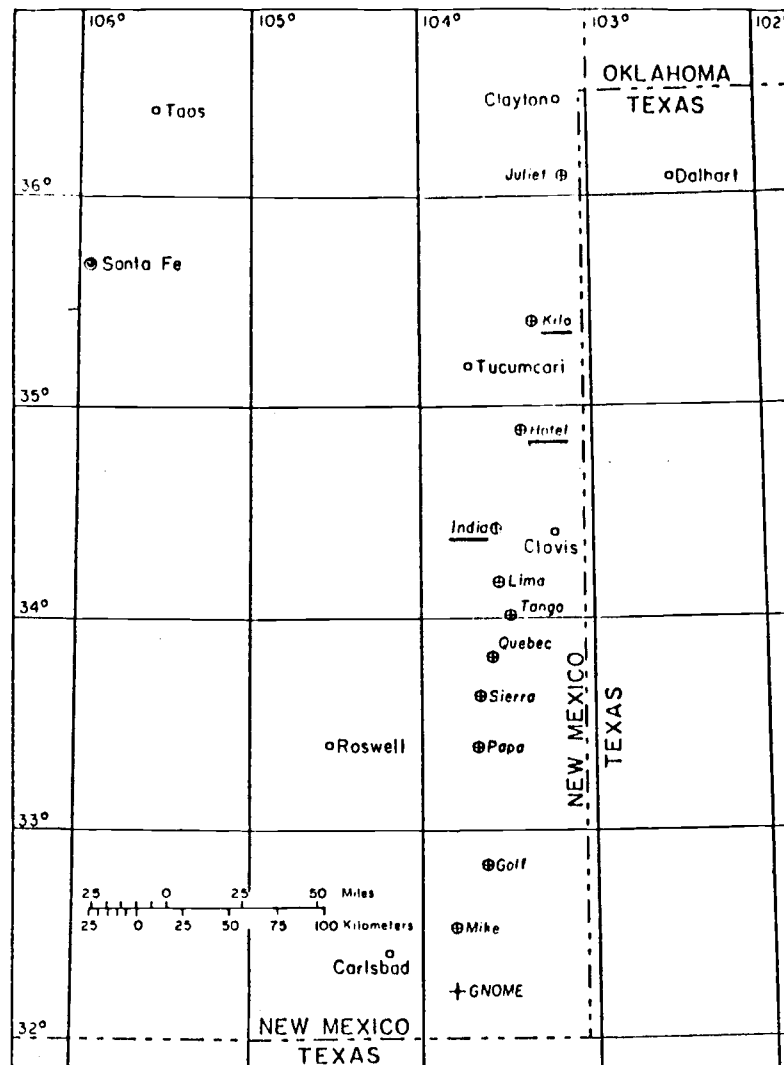


FIG. 1. Index map showing seismic recording locations for the GNOME explosion. *

Explanation: ⊕ = Seismic recording station

○ = City

*(16, p. 1019)

The seismometer arrays at each station consisted of six vertical component seismometers at 0.5 km. intervals in line with the explosion, but only four vertical component seismometer traces were available for interpretation (16, p. 1020). One radial and one transverse horizontal seismometers were used together with one of the vertical instruments at each recording station. The refraction system used at all the stations consisted of Hall-Sears (HS-10) seismometers and the U. S. Geological Survey's amplification system described in the literature (18). The electrical signal from each of the six seismometers was recorded on two different traces which differed in level by 15 decibels. At all stations, the higher level recording was used in this research.

Figures 2a, b and c show tracings of the records used for this research and hodographs of the ground motion. The hodographs show vertical versus radial horizontal ground motion for equal increments of time. For a compressional wave, the ground motion would move between the first and third quadrants in a push-pull motion (see Figure 2a). The hodographs were used to determine the extent to which the recorded traces were compressional waves. Figures 2a and 2c show that the first recorded traces were compressional, whereas, Figure 2b does not show this. Stewart and Pakiser (16, p. 1026), however, reported that the first seismic arrivals for these recordings were compressional, so it was assumed that some error

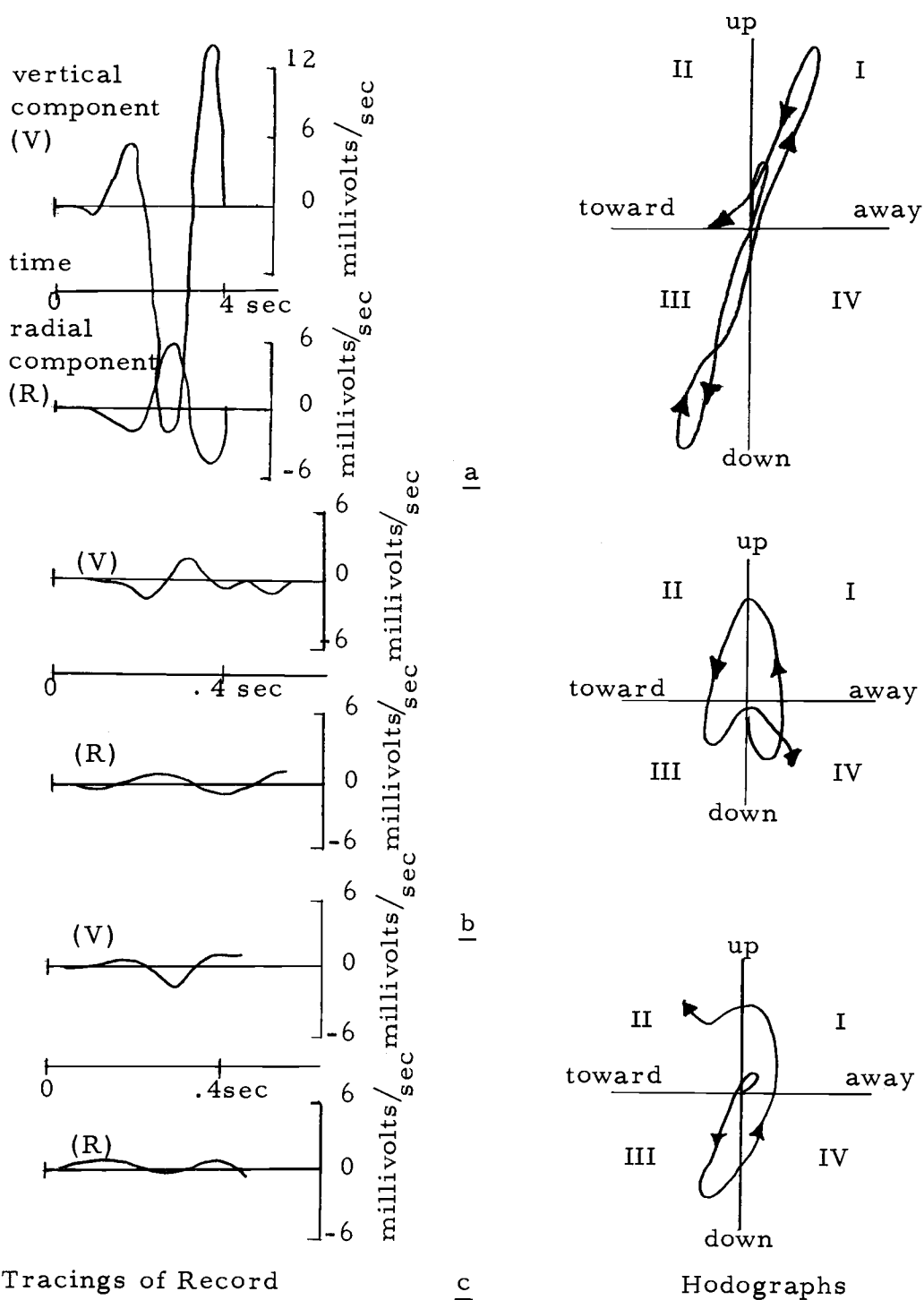


Figure 2. Tracings of Records of Ground Motion Used in This Research and Hodographs Showing Character of Ground Motion.

a) INDIA, 245 km. b) HOTEL, 300 km. c) KILO, 355 km.

had been made in the electrical connection for Figure 2b (station HOTEL).

The recorded ground motions shown in Figures 2a, b and c result from photographically recording light beam reflections from galvanometers which respond to the voltage output from the seismometer-amplifier systems. Thus, the trace deflections are proportional to the voltages applied to the galvanometers by the seismometer-amplifier units. The recorded ground motion traces in the above figures were digitized at intervals of 0.0159 seconds using a traveling microscope. The digitized trace amplitudes were converted from centimeters to millivolts using the constants given in Table II. The calibration data were furnished with the seismograms by the U. S. Geological Survey. In Table II, A, B, C and D refer to the vertical instruments at each station and E to the radial horizontal.

The digitized trace amplitudes had units of millivolts. The time functions of the digitized amplitudes were transformed into the frequency domain by means of the Fourier transform:

$$g(\omega) = \frac{1}{2\pi} \int_{-\infty}^{\infty} f(t)e^{-i\omega t} dt \quad (1)$$

where: $g(\omega)$ = the transform of $f(t)$

$f(t)$ = the time function of the seismogram trace

$$i = (-1)^{\frac{1}{2}}$$

ω = angular frequency

Table II. Calibration of Amplifier and Recording Oscillograph for Frequencies from 1 to 30 cps.

Station		Calibration constant in millivolts/cm trace deflection
INDIA	A	5.038
	B	5.347
	C	5.348
	D	4.141
	E	4.237
HOTEL	A	2.714
	B	6.550
	C	6.944
	D	6.572
	E	3.415
KILO	A	4.878
	B	2.649
	C	3.697
	D	6.849
	E	4.815

In order to use the Fourier transform for the data of this research, a numerical approximation of equation (1) had to be derived. The method used in this research was to assume that the function between any two points t_1 and t_2 was a rectangular pulse, namely:

$$f(t) = \frac{f(t_1) + f(t_2)}{2} \quad t_1 < t < t_2$$

Thus, the entire range of digitized values consisted of a series of

rectangular pulses. When the integration of the Fourier transform is carried out using the above assumptions, the integral is approximated by a summation (see Appendix II for derivation).

Equation (1) was numerically integrated to yield amplitude and phase information for a frequency range between 1 and 30 cps, where:

$$g(\omega_k) = a_k + ib_k = \left| g(\omega_k) \right| e^{i\theta_k} \quad (2)$$

$$\left| g(\omega_k) \right| = (a_k^2 + b_k^2)^{\frac{1}{2}}$$

$$\theta_k = \tan^{-1} \left(b_k / a_k \right)$$

Figure 3 shows a plot of amplitude, $\left| g(\omega) \right|$, versus frequency for the trace motion recorded at station KILO.

The amplitude and phase information for all recorded data were corrected for instrument response. A theoretical equation for the response of the seismometers to ground motion was developed by Dr. J. P. Eaton, U. S. Geological Survey (7). The equation was solved to give the phase response of the instruments to simple harmonic ground particle velocity (see Appendix I). Figures 4a and 4b give the theoretical amplitude and phase response of the seismometers. Figures 5a and 5b give the response characteristics of the amplification and recording systems (courtesy of the U. S. Geological Survey).

The recorded ground motions corrected for seismometer,

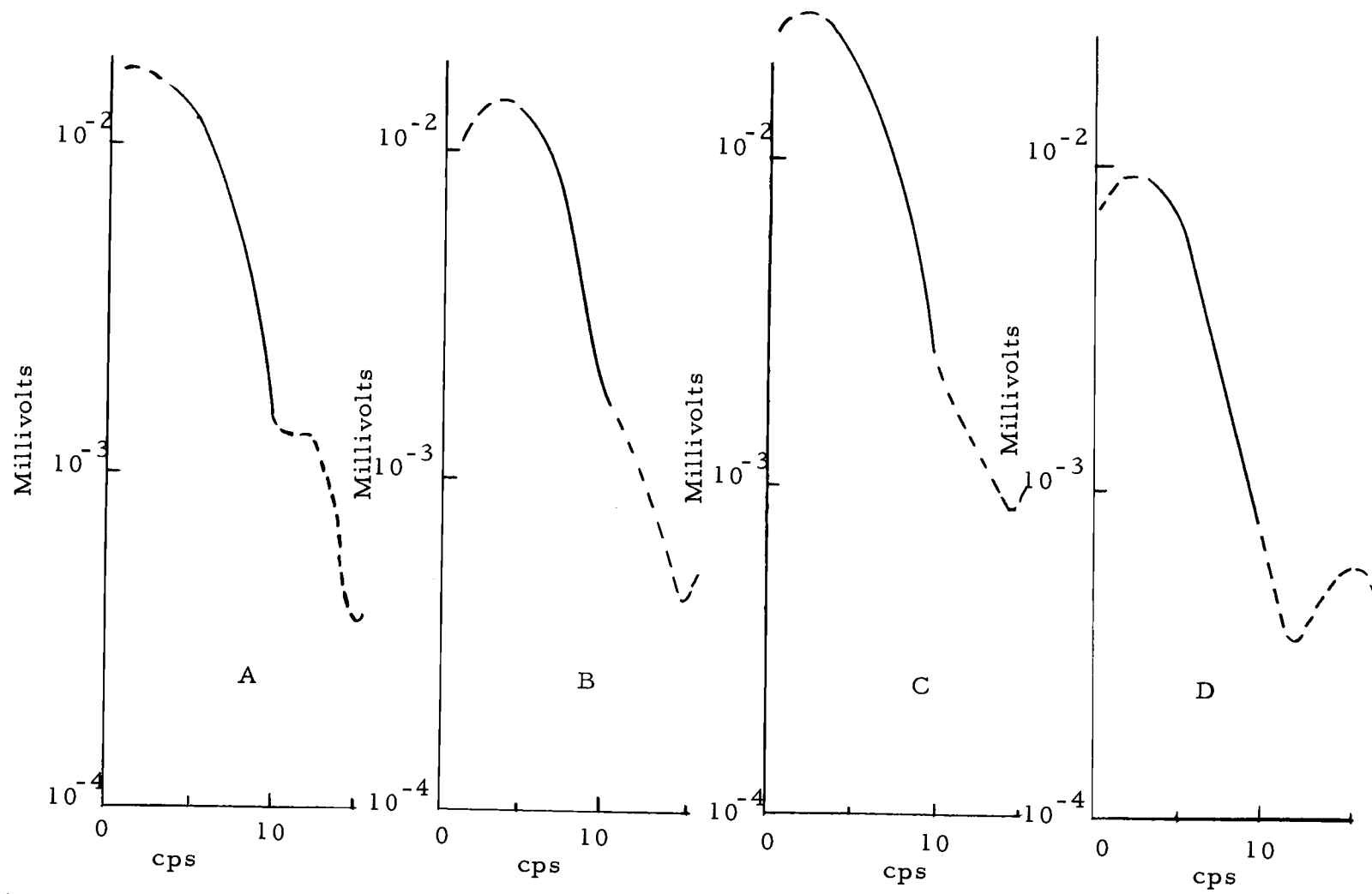


Figure 3. Frequency Spectrum of Vertical Component of Trace Motion as Recorded at Station KILO.

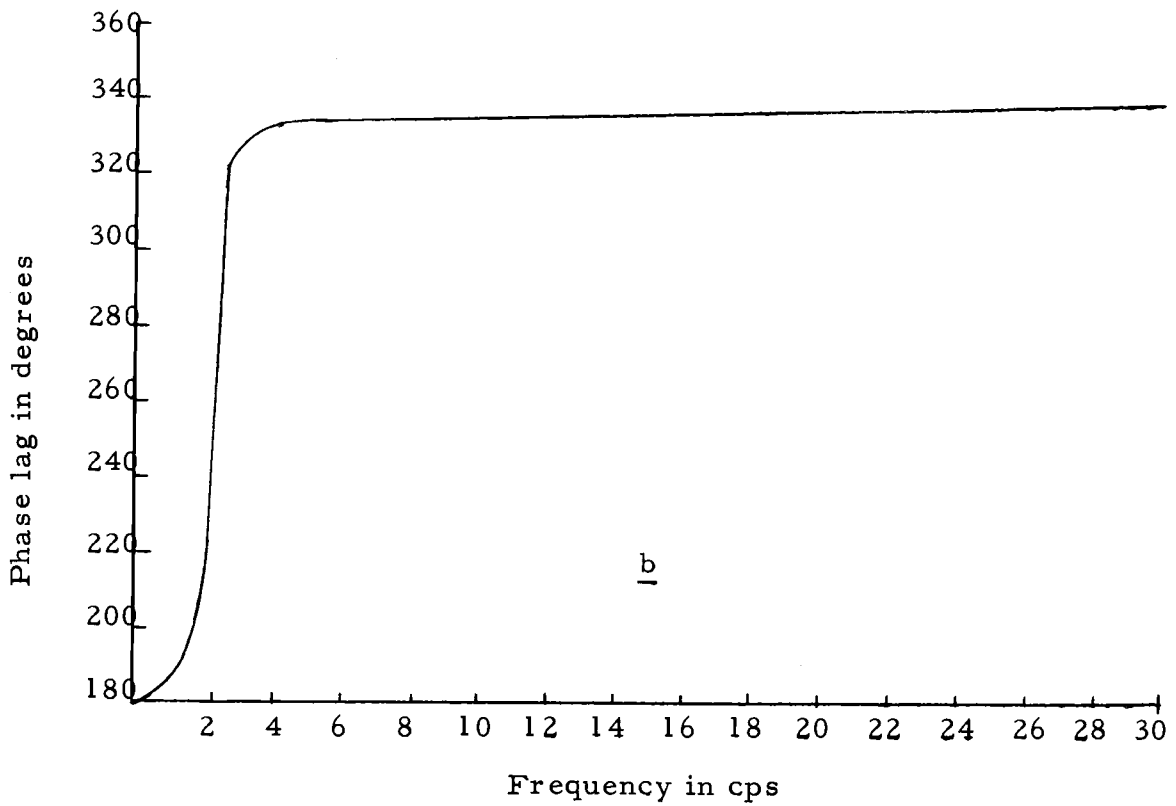
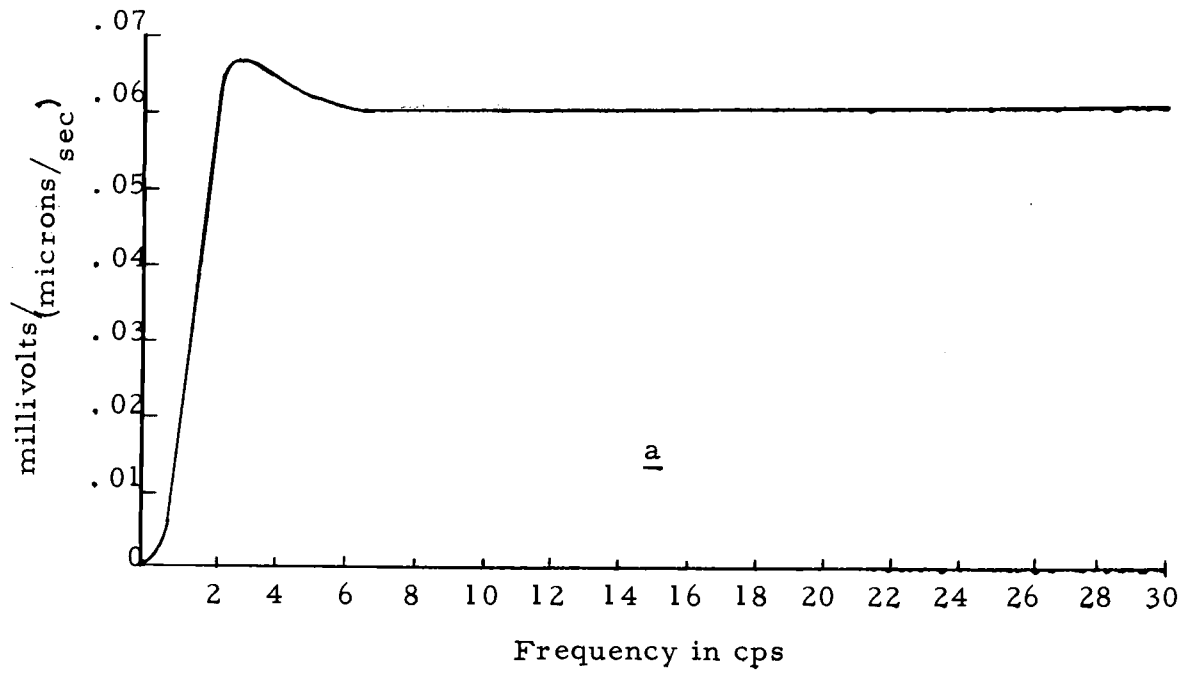


Figure 4. Theoretical Instrument Response Characteristics for Hall-Sears (HS-10) Seismometers.
a) amplitude response b) phase response

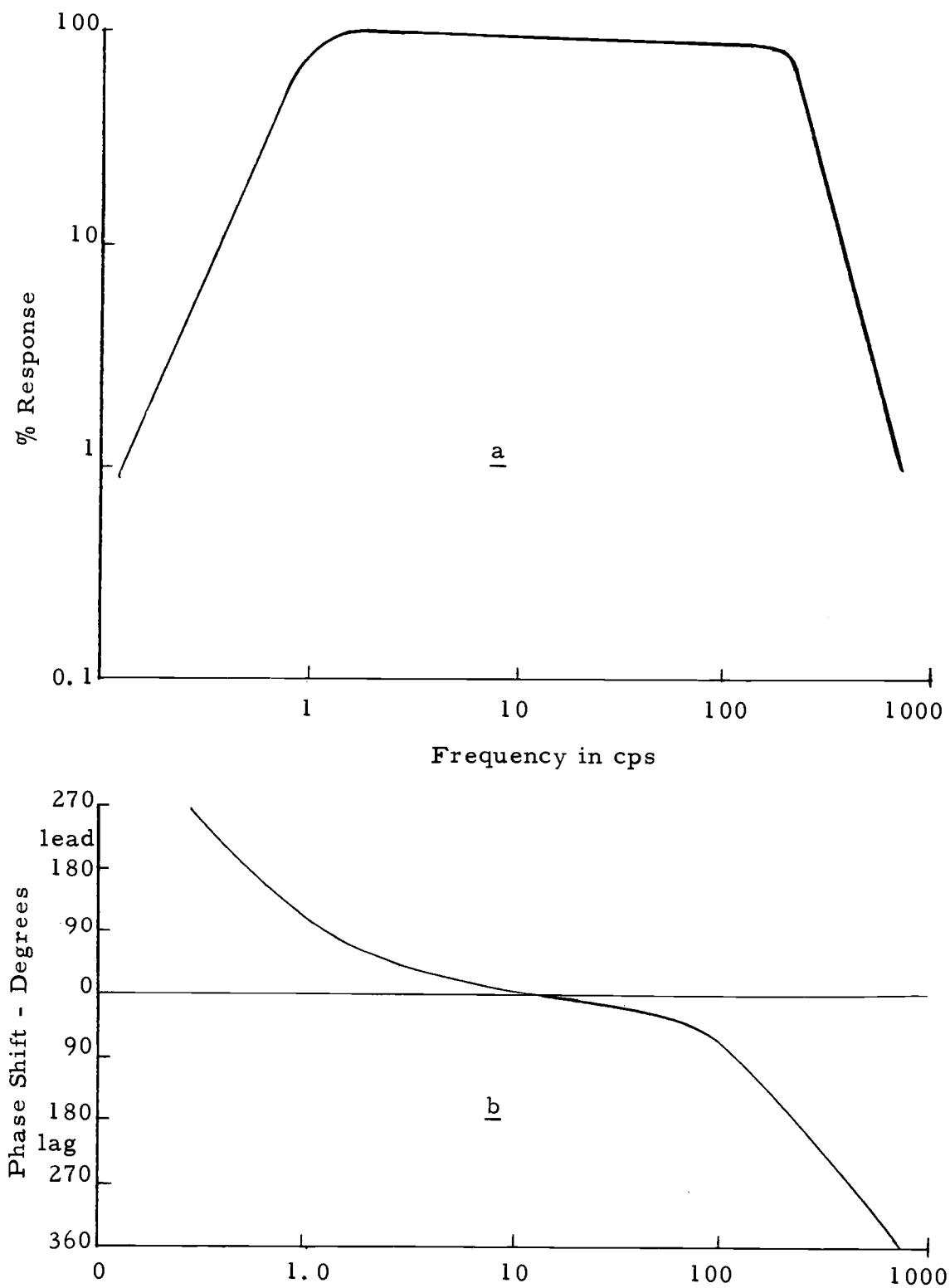


Figure 5. Response Characteristics of Amplification and Recording System a) amplitude response b) phase response

amplifier, and recording oscilloscope response were used in this research. The error involved in using a theoretical equation for the seismometer response is not known. However, all frequency spectra for ground motion were mathematically filtered to pass only frequencies between 3 and 10 cps. It is felt that the theoretical equation probably approximates the actual seismometer response in this range of frequencies. The filtering will be discussed further in the next section of this thesis.

ANALYSIS OF THE DATA

Seismogram traces recorded at INDIA, HOTEL and KILO were corrected for the response of the instruments as described in the last section. However, it was uncertain how much of the initial portion of the seismogram constituted the first compressional wave. To determine the pulse length, hodographs (see Figures 2a, b and c) were plotted to see when ground motion deviated from that characterized by compressional waves. From these studies, it was found that the first cycle of motion was largely compressional, but deviations from this type motion were involved soon after the first cycle or possibly during it. Further, the ground motion represented by the first cycle of the trace motion corresponds to the ground motion near the source as given by Berg, Trembly and Laun (3). This portion of the seismogram trace was used as the record of the compressional wave at all stations.

The compressional pulses were frequency analyzed as discussed in the last section, and the spectra were mathematically filtered. Frequencies greater than 10 cps and less than 3 cps were deleted. An analysis of the seismograms used in the research indicated that the frequency of the noise preceding the first arrival of seismic energy was about 12 cps and higher. Further, it was felt that the seismometer response data below 3 cps (see Figures 4a and 4b) were

more uncertain than that above this frequency. Hence, the pass-band was considered to be 3 to 10 cps in this research. It should be noted that the peak of the velocity spectrum for the ground motion recorded at 298 meters from the GNOME explosion occurs in this pass-band (see Figure 7e).

In order to go from the particle velocity spectrum, corrected for the recording instrument, to the confined particle velocity beneath the surface of the ground, it is necessary to correct the measured ground motion for the effects of the free surface. The emergence angles used for this correction were computed using the crustal model given by Stewart and Pakiser (16). A summary of the crustal model is given in Table III.

Table III. Crustal Model*

Layer	Thickness km	Compressional wave velocity km/sec	Shear wave velocity km/sec	Density** gm/cc	Cross-over distance km
1	4.2	4.92	2.89	2.60	25.2
2	15.0	6.14	3.61	2.65	151.6
3	10.9	6.72	3.95	2.75	210.5
4	19.7	7.15	4.21	3.00	240.5
5	----	8.23	4.45	3.34	-----

* (16, p. 1024)

** (17, p. 1548)

The emergence angle calculated from this crustal model is $53^{\circ}.4$ for all stations, whereas, the angles calculated from the data using the method given by Bullen (6, p. 127) and the maximum amplitudes of the radial horizontal and vertical components are 72° , $83^{\circ}.4$ and $82^{\circ}.6$ for INDIA, HOTEL and KILO, respectively. Also, using Bullen's method and values of particle velocity amplitudes, $|g(\omega)|$, at a frequency of 5 cps, obtained from the spectra of the vertical and radial horizontal seismograms, emergence angles are 73° , $72^{\circ}.3$ and 89° for the three stations, respectively. The emergence angles calculated from the observed data are much larger than the angles calculated for the crustal model in both cases. However, the variation in the ratio of vertical surface amplitude to the confined incident amplitude is small for emergence angles between 53° and 89° as can be seen in Table IV. The variation in the ratio of horizontal surface amplitude to the confined incident amplitude is not small as can be seen in Table IV also.

The emergence angle calculated for the crustal model, $53^{\circ}.4$, was used in all the calculations since there is some question about the calculation of emergence angles from seismogram traces. In any case, the choice of emergence angle values was not critical in this research since only seismogram traces of vertical ground motion were considered as directly applicable to the problem.

Table IV. Amplitude Ratios of Vertical and Horizontal Surface Motion to Incident Compressional Motion for Different Angles of Emergence*

Emergence Angle	qz/q_i	qr/q_i
53°.4	1.92	1.25
83°.4	1.98	0.25
89°.0	2.00	0.01

where: qz = vertical surface amplitude
 qr = horizontal surface amplitude
 q_i = incident confined amplitude

* (10, p. 99)

After the recorded ground motion was corrected for the effects of the free surface, the spectrum was inversely transformed to give the derived confined ground motion using the equation:

$$f(t) = \int_{-\infty}^{\infty} g(\omega) e^{i\omega t} d\omega, \quad (3)$$

where: $f(t)$ = time function of the derived ground motion

$g(\omega)$ = frequency spectrum

$$i = (-1)^{\frac{1}{2}}$$

ω = angular frequency

The derivation of the inverse transform for digitized pulses is given in Appendix III.

Figures 6a, b and c give the confined ground particle velocity at the stations resulting from the inverse transformations of the data. The average first peak amplitude values for stations INDIA, HOTEL and KILO are 10.2, 15.8 and 6.3 microns/sec., respectively. These values compare favorably with those given by Stewart and Pakiser (16, p. 1026). Notice that the direction of first motion of the verticals for station HOTEL is reversed due, probably, to the cause mentioned previously (see p. 5). Station HOTEL was also hampered by a large amplitude phase arriving during the second half cycle of trace motion (16, p. 1027).

Changes in amplitude, other than at the free surface, can occur along the transmission path of the wave due to the following factors:

- 1) amplitude loss at each acoustic interface,
- 2) amplitude change due to critical refraction,
- 3) geometrical spreading of the wave, and
- 4) the absorption of energy along the ray path.

Each of these factors will be discussed below in the order given.

1) To account for energy losses at acoustic interfaces, transmission co-efficients were computed for the geological model using the graphs given by McCamy, Meyer and Smith (12, p. 927-955). These investigators used the Nafe-Drake velocity versus density relation (17, p. 1548) to apply the Zoeppritz equations for velocity ratios alone. The ratios of the velocities on either side of the

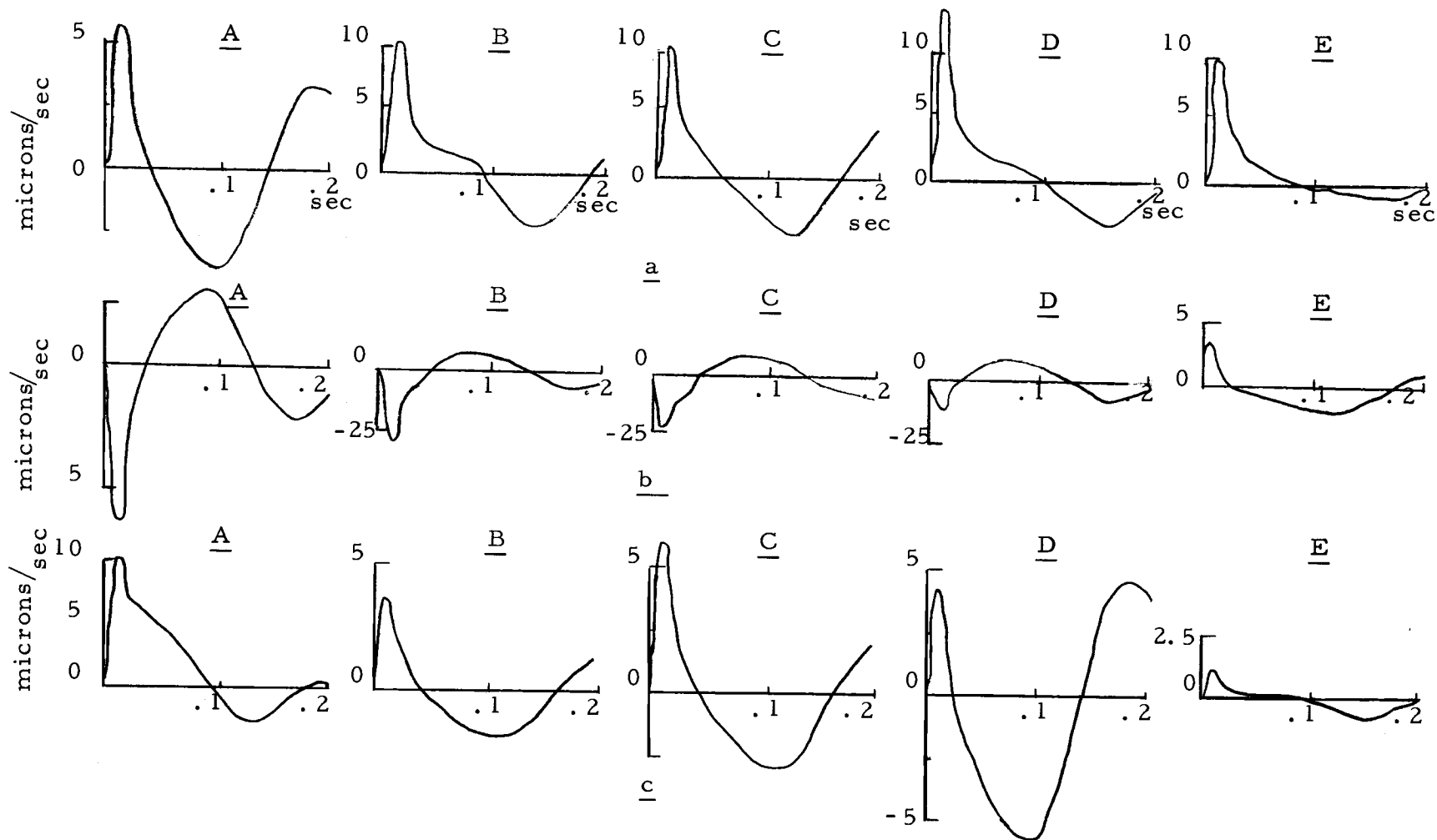


Figure 6. Derived Confined Motion of Ground in Microns/sec. for Frequencies 3-10 cps Using The First Cycle of Trace Motion.

a) INDIA

b) HOTEL

c) KILO

interfaces given in the crustal model were used together with the ray path angles to obtain the transmission co-efficients given in Table V.

Table V. Amplitude Ratio of Transmitted Compressional Wave to Incident Compressional Wave for Crustal Model Layers (12, p. 927-955)

Layer	Amplitude Ratio
Downward Path	(transmitted wave/incident wave)
1-2	0.90
2-3	1.00
3-4	1.02
Upward Path	
4-3	0.97
3-2	1.01
2-1	1.04

Thus, for any acoustic interface, the amplitude of the transmitted wave can be obtained by multiplying the incident wave by the amplitude ratio constant. Conversely, knowing the amplitude of the transmitted wave, the amplitude of the incident wave can be calculated. This method of correcting for boundary losses was used in this research.

2) The amplitude change due to a critical refraction (23, p. 6) for a two layered case is as follows:

$$q_H = A_{10}^* \frac{\gamma}{(1 - \gamma^2)^{1/2}} \frac{1}{R^{1/2} L^{3/2}} f(\Delta N), \quad (4)$$

where: $A_{10}^* \frac{\gamma}{(1 - \gamma^2)^{1/2}}$ = head co-efficient

q_H = displacement of head wave as recorded in the upper medium

R = epicenter distance

L = glide distance (distance of critical refraction)

$f(\Delta N)$ = reduced particle displacement potential

ΔN = $a_1 t - R$

a_1 = velocity in upper media

t = time

$$\phi = \frac{f(\Delta N)}{R} \quad (5)$$

ϕ = general particle displacement potential function for spherically diverging waves.

The head wave particle velocity in terms of the reduced particle displacement potential is as follows:

$$\dot{q}_H = A_{10}^* \frac{\gamma}{(1 - \gamma^2)^{1/2}} \frac{1}{R^{1/2} L^{3/2}} \frac{\partial f(\Delta N)}{\partial t}, \quad (6)$$

where: \dot{q}_H = particle velocity of head wave.

The particle velocity of the primary seismic compressional wave in terms of the reduced particle displacement potential is:

$$\dot{q}_B = \frac{\partial}{\partial r} \frac{\partial \phi}{\partial t} = \frac{-1}{R^2} \frac{\partial f(\Delta N)}{\partial t} + \frac{1}{R} \frac{\partial^2 f(\Delta N)}{\partial r \partial t} \quad (7)$$

\dot{q}_B = particle velocity of the primary seismic compressional wave.

Thus, the particle velocity of the primary seismic compressional wave should not, in general, compare with the particle velocity of the head wave either in form or in amplitude. However, the time differential of the particle displacement potential,

$$\frac{\partial \phi}{\partial t} = \frac{1}{R} \frac{\partial f(\Delta N)}{\partial t}, \quad (8)$$

which is the velocity potential for the primary seismic compressional wave, will have the same wave form as the head wave particle velocity but will differ in amplitude. Therefore, it is necessary to use the particle velocity potential of the primary seismic compressional wave to find the wave form of the head wave. Two cases of the velocity potential, $\frac{\partial \phi}{\partial t}$, were considered because it was unknown whether the wave form was distance dependent. Since the wave form of the initial seismic compressional wave and the head wave is governed by the reduced displacement potential, $f(\Delta N)$, the two cases are discussed below as Case I, where $f(\Delta N)$ is independent of distance, and Case II, where $f(\Delta N)$ is distance dependent.

Case I. Assuming that $f(\Delta N)$ is independent of distance in equation (7),

$$\frac{\partial^2 f(\Delta N)}{\partial r \partial t} = 0,$$

then equation (7) reduces to:

$$\dot{q}_B = \frac{-1}{R^2} \frac{\partial f(\Delta N)}{\partial t}, \quad (9)$$

and

$$\frac{\partial \phi}{\partial t} = \frac{1}{R} \frac{\partial f(\Delta N)}{\partial t} = -R \dot{q}_B. \quad (10)$$

Thus, the amplitude of the velocity varies with epicentral distance, but the wave form is unchanged because no phase change is involved in equation (9). The velocity potential for this case was calculated using the particle velocity measured at 298 meters from ground zero (see Figures 7a, b and c). According to O'Brien (13, p. 233), the polarity of the head waves should be the same as the direct compressional wave. Hence, the negative plot of the filtered potential is shown in Figure 7d. If the waves recorded at distance are head waves and if the reduced velocity potential is distance independent, then the recorded waves should compare favorably with Figure 7d when reduced to the source.

Case II. The potential function used for this case [$f(\Delta N)$ is distance dependent] was given by Blake (4, p. 213) and the values of the variables of the potential function by Berg and Papageorge (2, p. 949). The particle velocity and the velocity potential are shown in Figures 8a, b and c. A negative plot of the filtered potential is shown in

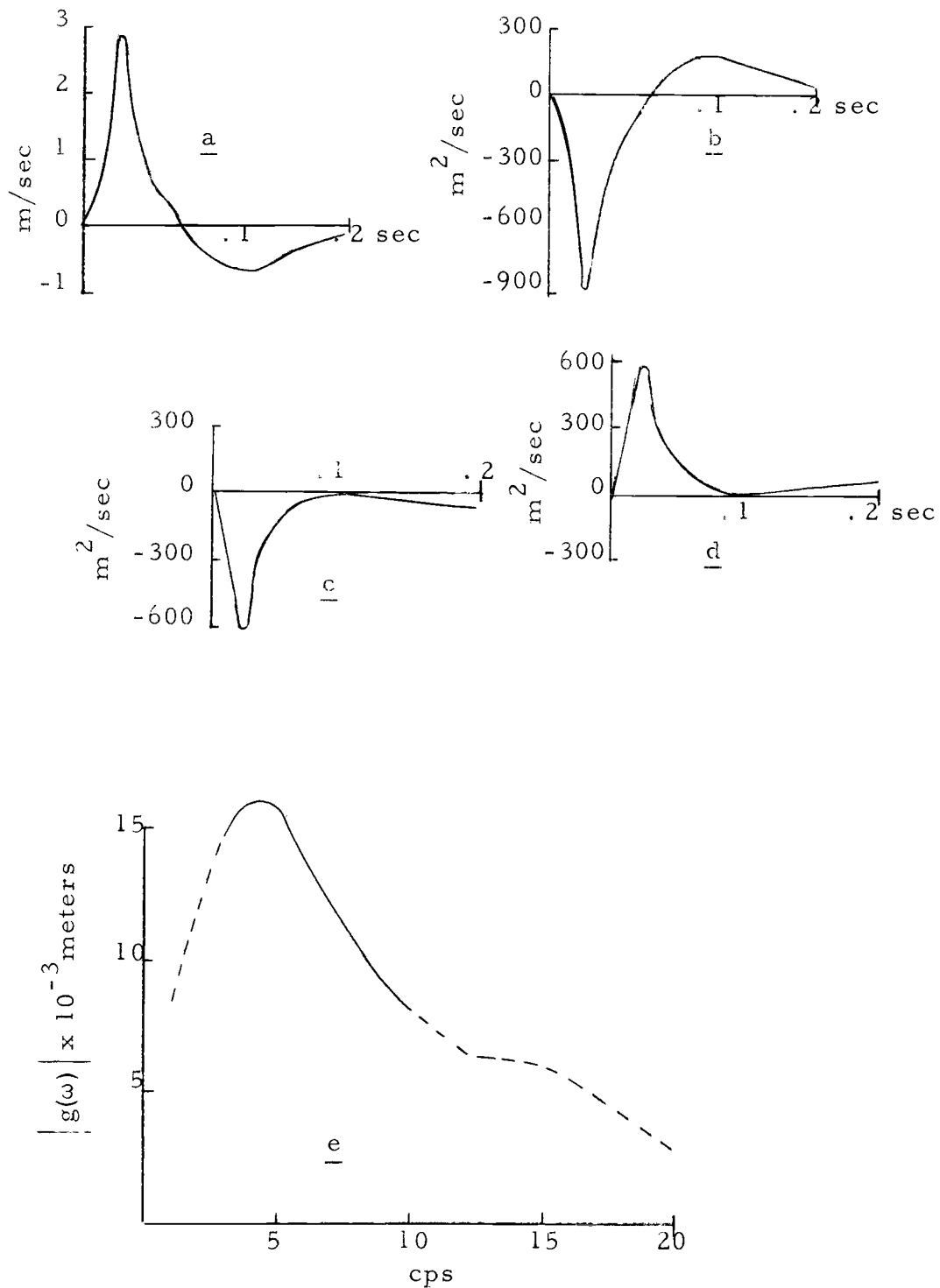


Figure 7. Graphs of Velocity Potential, Velocity and Frequency Spectrum of Case I. a) particle velocity measured at 298 m from source, b) unfiltered velocity potential at 298 m, c) velocity potential filtered 3-10 cps at 298 m, d) negative of filtered velocity potential at 298 m, e) spectrum of measured particle velocity.

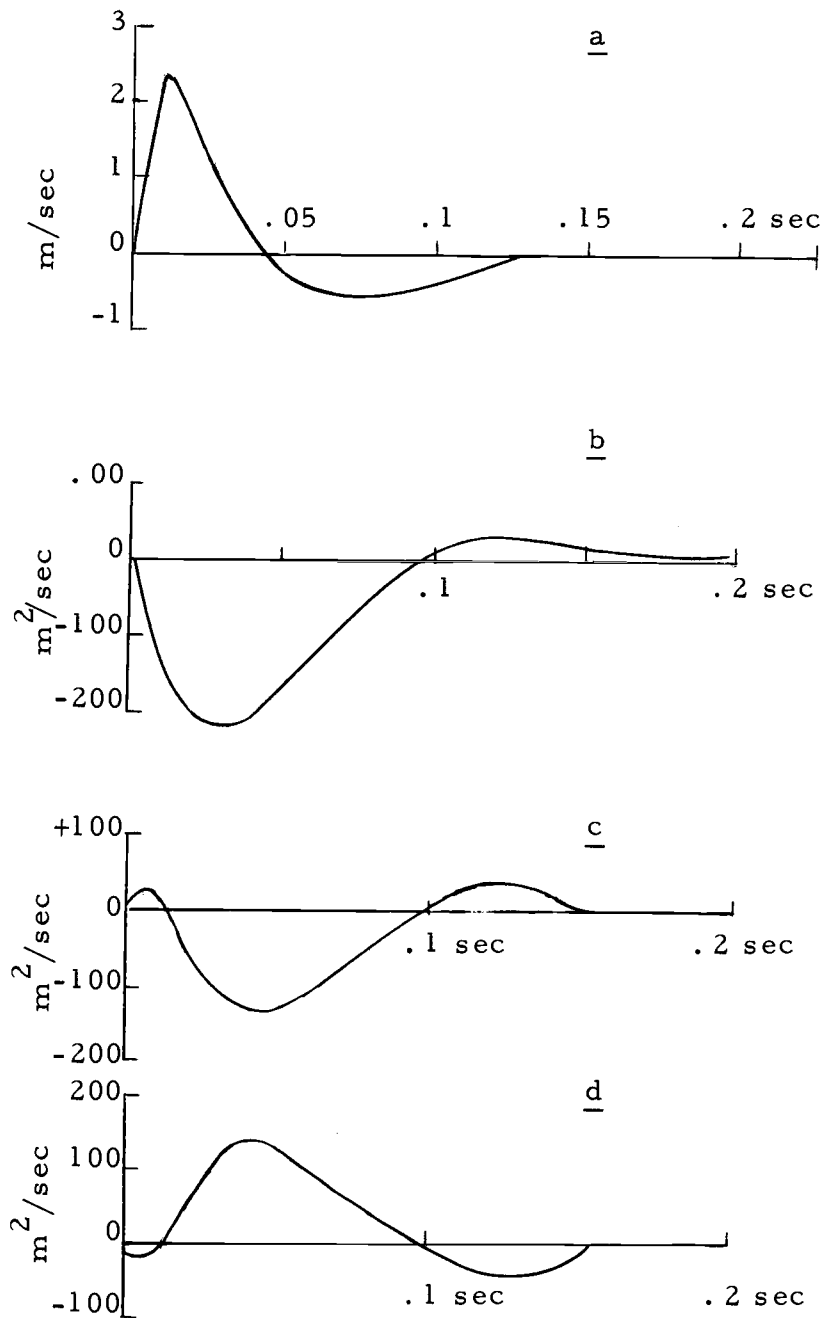


Figure 8. Graphs of Velocity Potential and Particle Velocity.
Case II.

- a) body velocity at 298 m.
- b) velocity potential at 298 m.
- c) velocity potential at 298 m filtered 3-10 cps.
- d) negative of filtered velocity potential at 298 m.

Figure 8d (13, p. 233). Thus, if the waves recorded at distance are head waves and if the reduced potential is distance dependent, then the recorded waves should compare favorably with Figure 8d.

The head co-efficient, $A_{10}^* \frac{\gamma}{(1 - \gamma)^2}$ for the transmission path

along the base of the crust, was computed (see Werth, Herbst and Springer, 20, p. 1592, for equations) using the curve of Nafe-Drake (17, p. 1548), and assuming Poisson's ratio to be 0.25,

$$V_p = 1.732 \times V_s$$

where: V_p = compressional wave velocity

V_s = shear wave velocity

3) The head wave equation (6) assumes a two-layered media, but the crustal model used consists of five layers. The three additional layers affect the spherical spreading of the wave. This effect has been offset by using a virtual source which is the same technique used by Werth, Herbst and Springer (20, p. 1592).

The virtual source, in essence, replaces the original source and is located such that it gives the same energy and amplitude at the point of critical refraction as the original source. However, the distance to the virtual source from the point of refraction is different than that of the original source. (Appendix IV gives a graphical derivation of the virtual source.) The change in epicentral distance due to the change to a two-layered case is simply the difference in

horizontal distance between the ray path for the two models (20, p. 1595). The epicentral distance correction for this research was calculated to be -3.2 km.

4) To account for energy lost by absorption along the transmission path, a theoretical equation given by Futterman (8, p. 5279) was used in this research. A summary of the development of this equation follows.

Given the wave equation:

$$u(R, t) = u_o \exp\left(\frac{-\omega R}{2cQ} (1 - e^{-x}) + i\phi\right) \cdot \exp(-i\omega t). \quad (11)$$

where: $u(R, t)$ = amplitude at distance R

u_o = initial amplitude

ω = angular frequency

c = non-dispersive phase velocity

Q = attenuation constant

x = ω/ω_o

ϕ = $\frac{\omega R}{V_p}$

$V_p = c\left(1 - \frac{1}{\pi Q} \ln x\right)^{-1}$

ω_o = cut-off frequency (very low)

R = epicenter distance

t = time

$i = (-1)^{\frac{1}{2}}$

Since ω_0 was given by Futterman (8, p. 5286) as $2\pi \cdot 10^{-3} \text{ sec}^{-1}$, $x \geq 15$ for the frequencies used (3 to 10 cps), and the amplitude attenuation is approximated by the term

$$\exp\left(\frac{-\omega R}{2cQ}\right). \quad (12)$$

Since

$$\left(1 - \frac{1}{\pi Q} \ln x\right)^{-1} \simeq 1, \\ V_p \simeq c,$$

and the phase is approximated by the term

$$\exp\left(\frac{i\omega R}{c}\right). \quad (13)$$

The wave equation (11), using equation (12) and (13), reduces to

$$u(R, t) \simeq u_0 \exp\left(\frac{-\omega R}{2cQ}\right) \exp\left(\frac{i\omega R}{c} - i\omega t\right). \quad (14)$$

Equation (14) describes a non-dispersive wave (6, p. 58), because the phase velocity is no longer a function of frequency. However, the exact equation would involve slight dispersion, but the data did not warrant this refinement.

The attenuation factor, equation (12), contains a constant Q that depends on the propagation path. An attempt was made to determine Q from the data but this proved unsatisfactory. Further, a literature search was made to obtain additional information about the attenuation, and values of Q used by other investigators were found that varied from 200 to 2500 for compressional waves in the upper portion of the earth (20, p. 1607; 21, p. 1469; 11, p. 190; 5, p. 84).

Values of Q of 250, 500 and 800 were used in this research. The exact value of Q that actually pertains to the transmission path is not known.

In summary for head waves, the entire calculation for reducing the recorded ground motion at distance to the near source region consists of an inverse transform [equation (3)] of the following product:

$$G(\omega) = \frac{g(\omega)}{K \cdot A(\omega)} \quad (15)$$

where: $G(\omega)$ = frequency dependent function in equation (3)

$g(\omega)$ = spectrum of the measured ground particle velocity at each station

K = product of all the non-frequency dependent terms which are:

- 1) free surface motion to confined ground motion constants for $53^\circ.4$ (Table IV);
- 2) transmission co-efficients listed in Table V;
- 3) the head co-efficient including the geometrical spreading term,

$$\frac{1}{R^{1/2}L^{3/2}} ;$$

- 4) ratio of virtual source to actual source (Appendix IV);

$A(\omega)$ = amplitude attenuation [equation (12)].

Figures 9, 10 and 11 show the calculated source potentials for ground motions recorded at INDIA, HOTEL and KILO using the method of calculation described above.

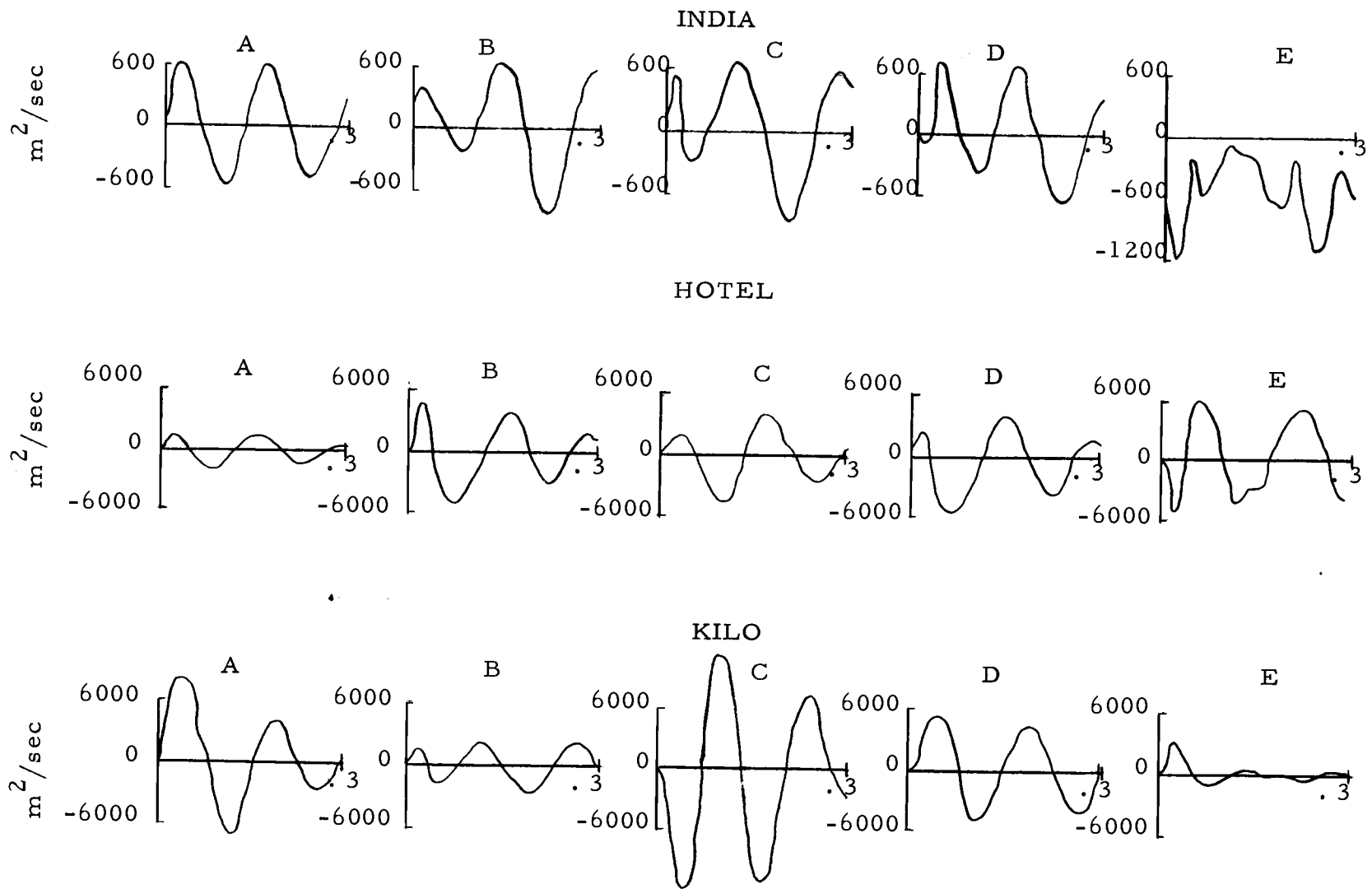


Figure 9. Filtered Calculated Source Potentials for $Q = 250$ (amplitudes in m^2/sec).

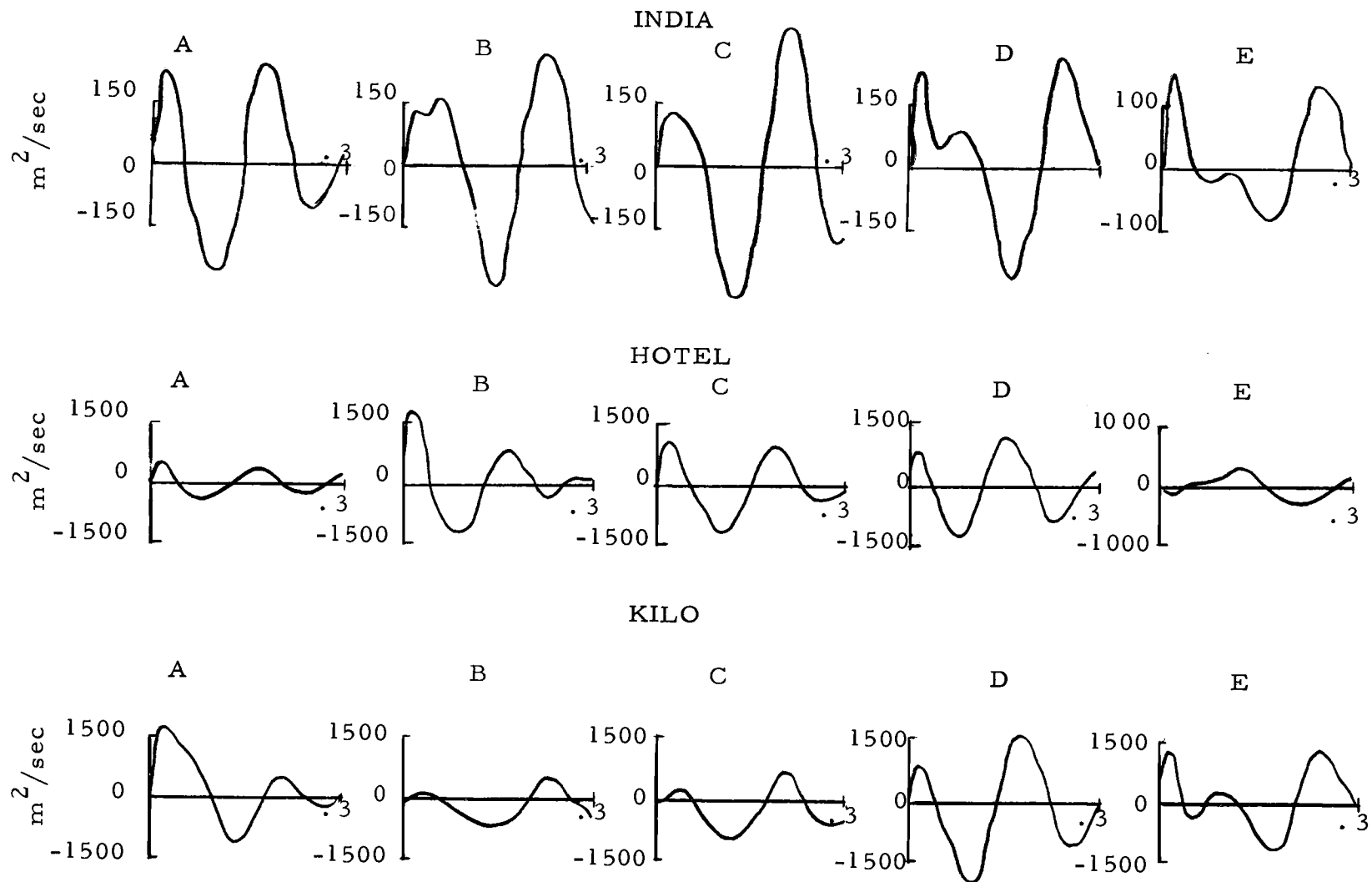


Figure 10. Filtered Calculated Source Potentials for $Q = 500$ (Amplitudes in m^2/sec)

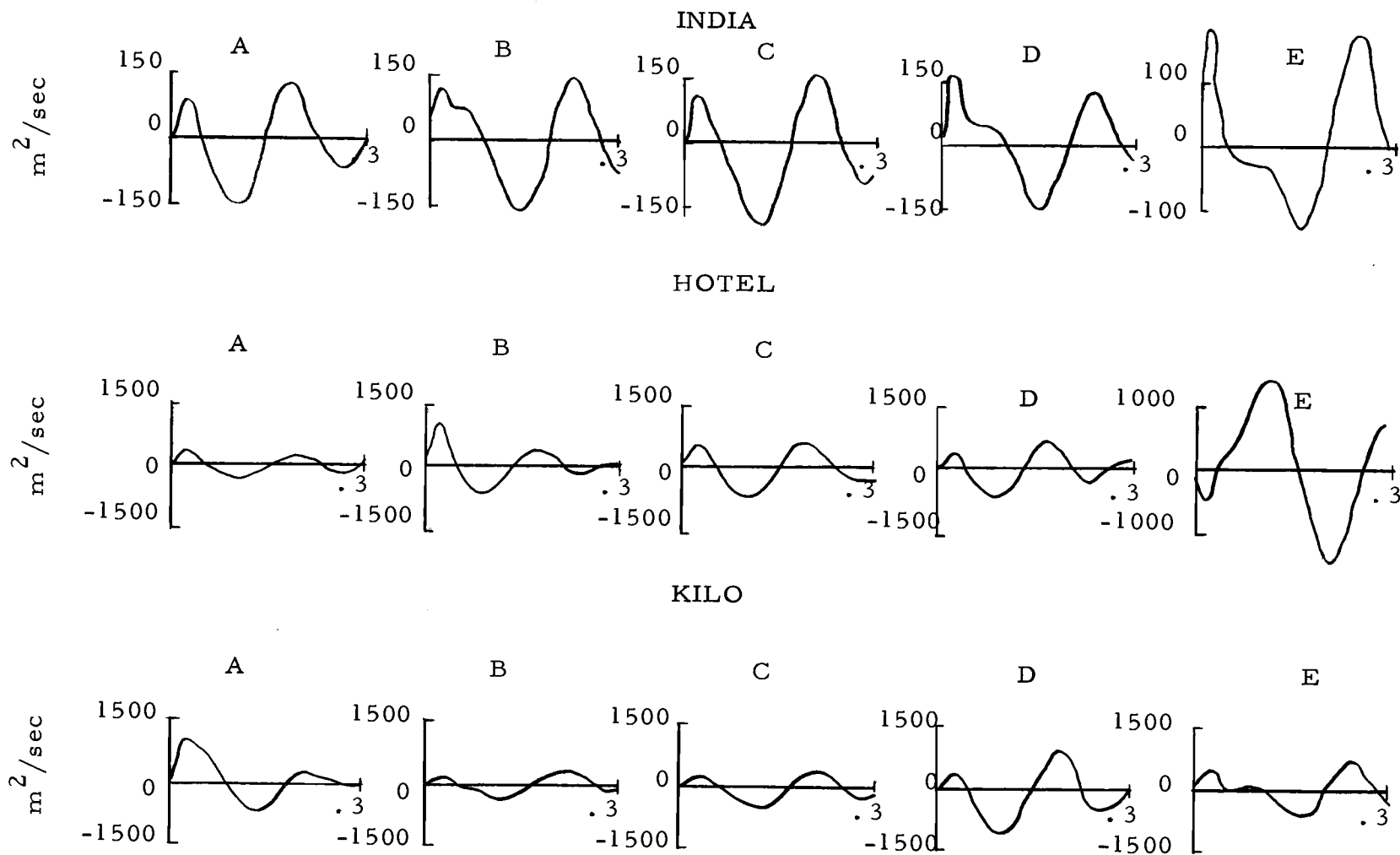


Figure 11. Filtered Calculated Source Potential for $Q = 800$ (amplitudes in m^2/sec)

DISCUSSION OF RESULTS

If the distant seismic signals were head waves and if instrument response characteristics and all the assumptions concerning the geological model were correct, then one set of calculated source potentials shown in Figures 9, 10 and 11 would be expected to compare in both form and amplitude with either the Case I, Figure 7d, or the Case II, Figure 8d, potential. A comparison between Figures 9, 10 and 11 and Figures 7d and 8d shows neither Figures 7d or 8d have the large overshoot and return of the potentials of Figures 9, 10 and 11. The average period of the first half cycle is 0.06 seconds for Figures 9, 10 and 11, whereas, the period of the first half cycle of Figure 7d (when extended to the axis) and Figure 8d (ignoring the first small half cycle) is about 0.08 seconds. Thus, the source potentials in Figures 7d and 8d have a lower frequency content than those of Figures 9, 10 and 11.

Table VI gives a comparison of the first peak amplitudes for the calculated source potentials, Table VI A, with the first peak amplitudes of Cases I and II source potentials (ignoring the initial small half cycle of Figure 8d), Table VI B. The first peak amplitudes of the calculated source potentials for all seismometers at the stations were averaged to obtain the values given in Table VI A. If a direct comparison can be made between the amplitudes of Figure 8d and

Figures 9, 10 and 11, it would appear that the value of Q for the propagation path would be about 500. Thus, if the distant seismic signals are head waves, the reduced displacement potential would be distance dependent since it would compare to Case II in amplitude.

Table VI. Averaged First Peak Amplitudes for the Calculated Source Potentials for INDIA, HOTEL and KILO Compared with First Peak Amplitudes for Case I and Case II Potentials (all in $m^2/sec.$)

<u>Station</u>	Q	A		
		250	500	800
INDIA		577.	135.	130.
HOTEL		3000.	1050.	547.
KILO		2660.	375.	187.5
- - - - -				
		B		
Case I (Figure 7d)			600. $m^2/sec.$	
Case II (Figure 8d)			140. $m^2/sec.$	

The variation in first peak amplitudes for stations INDIA and KILO is not completely understood, but such factors as local geology at the recording site, variation of individual instrument responses, possible interference with the first compressional motion by other waves, and incorrect propagation path and absorptive attenuation descriptions are important considerations. Additional research is needed to give a more complete comparison between the velocity potential at the source and the source velocity potential calculated from seismic

arrivals of assumed head waves measured at distances between 250 and 350 km.

If the ground motion measured at stations INDIA, HOTEL and KILO resulted from body wave propagation rather than head wave propagation, then the derived confined ground motion at these stations should compare with the particle velocity rather than the velocity potential.

In order to test the above hypothesis, the ground particle velocity at 300 km. was calculated using the equation given by Blake (see p. 23). The ground particle velocity, attenuated by spherical spreading only, is shown in Figure 12a, and filtered using a pass-band 3-10 cps in Figure 12b. The ground motion derived from seismogram traces and filtered with a pass-band of 3-10 cps is shown in Figure 6. The wave forms of Figure 6 and Figure 12b compare very well. However, the frequency content of the particle velocity calculated by the Blake equation is higher than that of the derived confined ground motion. No absorptive attenuation has been considered in this comparison.

In order to test further the body wave hypothesis it was necessary to construct another crustal model since the model by Stewart and Pakiser (16) permits only head waves as first arrivals at distances greater than 240 km. from the source. A crustal model with a constant velocity gradient which varied from 4.92 km/sec at the surface to 8.23 km/sec at 50.8 km. was used (16). Using the

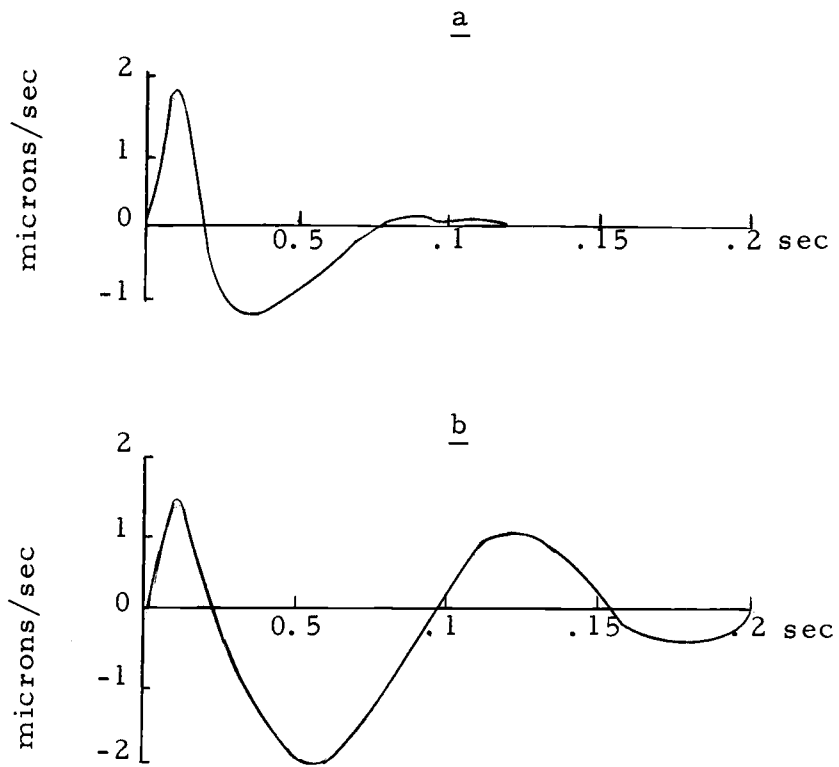


Figure 12. Body Velocity at 300 km. from Source Potential. Case II
a) body velocity as calculated
b) body velocity, a, filtered 3-10 cps

equations given by Officer (14, p. 59-61), the ray paths for this model have a maximum depth of penetration of 117 km. and travel path distances from the source to stations INDIA, HOTEL and KILO are 295, 377 and 450 km., respectively. A simplified equation for amplitude decrease with distance is given by:

$$V = \frac{V_o}{R} e^{-\alpha R} \quad (16)$$

where: $R = r^n$

V = velocity amplitude at distance

V_o = initial velocity (3.0 m/sec)

R = ray path distance

r = epicenter distance

α = attenuation constant

n = geometrical spreading constant.

Using the average values of the amplitudes of derived confined particle velocities at INDIA and KILO and the velocity measured at 298 meters from the source, the attenuation constant (α) was computed to be 4.46×10^{-4} /km. For this model, curved ray path theory would apply and the amplitude would diminish as the epicenter distance, r^{-n} , where n is 1.20. The frequency dependency of α was not investigated.

The above body wave model probably represents the maximum

simplest linear velocity gradient that would pertain to this region. On the other extreme, the minimum simplest velocity gradient to be expected would be about 5.27×10^{-2} /sec (surface velocity of 4.92 km/sec and velocity of 7.6 km/sec at 50 km. depth). For this model, the maximum depth of penetration of the ray path is 108 km. and the travel path distances from the source to stations INDIA, HOTEL and KILO are 282, 361 and 436 km., respectively. The attenuation constant (not frequency dependent) for this model is 8.13×10^{-4} /km. and the value of n is 1.15. For the above two cases, the propagated amplitude of the measured velocity at 298 meters would compare exactly with the average amplitudes at stations INDIA, HOTEL and KILO.

From the above data it is not possible to determine whether the energy was propagated in the form of a head wave or a body wave. In both instances, comparisons can be made between theory and observation that appear favorable. However, the head wave propagation appears to be more tenuous than the body wave propagation since it is based on a comparison with a source velocity potential that could change considerably with a different approximation of the Blake equation to the observed velocity at 298 meters and the filtering of the potential derived from that velocity.

The velocity models and attenuations for the body wave propagation are simple and do not completely apply to the region. However, it is felt that the body wave type of propagation has to be

considered. The comparisons between the body wave propagation and the measured waves appear to be very good.

From the above discussion, a mode of propagation has to be more completely established before source information can be determined from ground motions measured at distance. For investigations such as those conducted for this thesis, more control is needed when obtaining the experimental data. For example, it is very important to have accurate calibration data for the instruments, accurate local geological information in the vicinity of the stations, accurate crustal and velocity models and sufficient measurements to obtain a representative sampling.

SUMMARY

In this research, measurements of the first arrivals of seismic waves at distances of 245 to 355 km. from the GNOME nuclear explosion were used to determine whether compressional wave characteristics at 298 meters from the source could be determined from the distant field signals. To do this, two modes of propagation of the wave were considered.

First, the compressional wave was assumed to be propagated as a head wave. The crustal model given by Stewart and Pakiser (16) was used for geological control. It was found that under very restricted conditions, the head wave propagation could possibly describe the mode of propagation, but the potentials for the measured wave at 298 meters from the source were not described adequately by the distant field measurements when they were reduced to 298 meters by this mode.

Second, the compressional wave was assumed to be propagated as a body wave. A compressional wave describing ground motion at 298 meters was propagated to 300 km. from the source considering geometrical spreading only. Wave characteristics of this signal compared very well with those measured at distances of 245 to 355 km.

From these two comparisons, it would seem possible that the waves measured at 245 to 355 km. from the source may be body waves

rather than head waves. More research is needed to make a conclusive choice between the two modes of propagation, and thus be able to determine near source wave characteristics from distant field measurements. However, methods were established in this research which will enable source motion to be described from distant measurements of a seismic signal when the data are sufficient to do so.

BIBLIOGRAPHY

1. Berg, J. W. Jr. and Kenneth L. Cook. Energies, magnitudes and amplitudes of seismic waves from quarry blasts at Promontory and Lakeside, Utah. *Bulletin of the Seismological Society of America* 51:389-399. 1961.
2. Berg, Joseph W. Jr. and George E. Papageorge. Elastic displacement of primary waves from explosive sources. *Bulletin of the Seismological Society of America* 54:947-959. 1964.
3. Berg, Joseph W. Jr., Lynn D. Trembly and Philip R. Laun. Primary ground displacements and seismic energy near the GNOME explosion. *Bulletin of the Seismological Society of America* 54:1115-1126. 1964.
4. Blake, F.G. Jr. Spherical wave propagation in solid media. *The Journal of the Acoustical Society of America* 24:211-215. 1952.
5. Birch, F. and D. Bancroft. The effect of pressure on the rigidity of rocks. *Journal of Geology* 46:59-87, 113-141. 1938.
6. Bullen, K. E. An introduction to the theory of seismology. 2d ed. New York, Cambridge University Press, 1953. 296p.
7. Eaton, J. P. Determination of true ground amplitudes from C. S. Refraction Seismograms. Memorandum to The Record of U. S. Geological Survey. August 13, 1962. 6 numb. leaves.
8. Futterman, Walter I. Dispersive body waves. *Journal of Geophysical Research* 67:5279-5292. 1962.
9. Guilleman, E. A. Mathematics of circuit analysis. New York, Wiley, 1949. 590p.
10. Gutenberg, B. Energy ratio of reflected and refracted seismic waves. *Bulletin of the Seismological Society of America* 34:85-102. 1944.
11. Gutenberg, Beno. Physics of the earth's interior. New York, Academic Press, 1959. 240p.

12. McCamy, Keith, Robert P. Meyer and Thomas J. Smith. Generally applicable solutions to Zoeppritz' amplitude equations. Bulletin of the Seismological Society of America 52:923-955. 1962.
13. O'Brien, P. N. S. Model seismology--the critical refraction of elastic waves. Geophysics 20:227-242. 1955.
14. Officer, C. B. Introduction to the theory of sound transmission with application to the ocean. New York, McGraw-Hill, 1958. 284p.
15. Savaresnkii, E. F., S. A. Fedorov and B. V. Gogichaishvili. The determination of the actual motion of the ground and its spectrum from a seismogram. Bulletin of the Academy of Sciences of the U. S. S. R. Geophysics Series, 1963, p. 1340-1347. (Translated from Izvestia Akademii Nauk S. S. S. R., Ser Geofizicheskaja)
16. Stewart, S. W. and L. C. Pakiser. Crustal structure in eastern New Mexico interpreted from the GNOME explosion. Bulletin of the Seismological Society of America 52:1017-1030. 1962.
17. Talwani, M., G. H. Sutton and J. L. Worzel. A crustal section across the Puerto Rico trench. Journal of Geophysical Research 64:1545-1555. 1959.
18. Warrick, R. E., et al. The specification and testing of a seismic-refraction system for crustal studies. Geophysics 26:820-824. 1961.
19. Weart, W. D. Particle motion near a nuclear detonation in halite. Bulletin of the Seismological Society of America 52:981-1005. 1962.
20. Werth, G. C., R. F. Herbst and D. L. Springer. Amplitudes of seismic arrivals from the M discontinuity. Journal of Geophysical Research 67:1587-1610. 1962.
21. Werth, Glenn C. and Roland F. Herbst. Comparison of amplitudes of seismic waves from nuclear explosions in four mediums. Journal of Geophysical Research 68:1463-1476. 1963.

22. Zvolinskii, N. V. Reflected and head waves emerging at a plane interface of two elastic media, 1. Bulletin of the Academy of Sciences of the U. S. S. R. Geophysics Series 10:1-21. 1957. (Translated from Izvestia Akademii Nauk S. S. S. R. , Ser Geofizicheskaiia)
23. Zvolinskii, N. V. Reflected waves and head waves arising at a plane interface between two elastic media, 2. Bulletin of the Academy of Sciences of the U. S. S. R. Geophysics Series, 1958, p. 1-7. (Translated from Izvestia Akademii Nauk S. S. S. R. , Ser. Geofizicheskaiia)

APPENDICES

APPENDIX I

Starting with the initial equation given in the memorandum by

Dr. J. P. Eaton (7):

$$\ddot{z} + 2\beta\Omega_0\dot{z} + \Omega_0^2 z = -\omega^2 A \sin \omega t,$$

where: z = seismometer mass displacement with respect to the seismometer frame

Ω_0 = natural frequency of the seismometer

$A \sin \omega t$ = ground displacement function

β = damping constant

ω = angular frequency

Solving for z yields:

$$z = \frac{-\omega^2 A \sin \left[\omega t - \tan^{-1} \left(\frac{2\beta\omega\Omega_0}{\Omega_0^2 - \omega^2} \right) \right]}{[(\Omega_0^2 - \omega^2)^2 + 4\beta^2\Omega_0^2\omega^2]^{\frac{1}{2}}}$$

The input voltage to the transformer is:

$$e(t) = \frac{ZG}{R+r} \frac{dz}{dt},$$

where (7): Z = input impedance of the input transformer
(resistive at operating frequencies)

G = sensitivity of the seismometer

R = impedance of the circuit external to the seismometer
(resistive at operating frequencies)

r = resistance of the seismometer coil

Differentiating z with respect to t and solving for $e(t)$ yields:

$$e(t) = \frac{-ZG\omega^3 A \cos[\omega t - \tan^{-1}(\frac{2\beta\Omega_o\omega}{\Omega_o^2 - \omega^2})]}{(R+r) [(\Omega_o^2 - \omega^2)^2 + 4\beta^2\Omega_o^2\omega^2]^{\frac{1}{2}}},$$

and, since $-\cos(\theta) = \cos(\theta - \pi)$, then:

$$e(t) = \frac{ZG\omega^3 A \cos[\omega t - \{\pi + \tan^{-1}(\frac{2\beta\Omega_o\omega}{\Omega_o^2 - \omega^2})\}]}{(R+r) [(\Omega_o^2 - \omega^2)^2 + 4\beta^2\Omega_o^2\omega^2]^{\frac{1}{2}}}$$

The ground displacement is given as $A \sin(\omega t)$ and, therefore, the ground velocity is $\omega A \cos(\omega t)$. The amplitude magnification of this motion is (from the previous equation):

$$\frac{\omega^2 \frac{Z}{(R+r)} G}{[(\Omega_o^2 - \omega^2)^2 + 4\beta^2\Omega_o^2\omega^2]^{\frac{1}{2}}},$$

and the phase change is:

$$\theta = \tan^{-1}(\frac{2\beta\Omega_o\omega}{\Omega_o^2 - \omega^2}) + 180^\circ.$$

Substituting the values given in the memorandum (7) for the parameters yields:

$$\theta = 180^\circ + \tan^{-1} \left(\frac{2.12}{4.16 - f^2} \right) ,$$

and the amplitude magnification is:

$$17.2787 \left[(4.16 f^2 - 1)^2 + \frac{4.50}{f^2} \right]^{\frac{1}{2}} ,$$

where: $\omega = 2\pi f$.

APPENDIX II

Derivation of the Fourier Transform Approximation:

Given: A curve, $f(t)$, that is zero every where except over a finite interval where it consists of a series of digitized points, $f(t_i)$.

The form of the Fourier Transform used is:

$$g(\omega) = \frac{1}{2\pi} \int_{-\infty}^{\infty} f(t) e^{-i\omega t} dt .$$

Approximate $f(t_i)$ by a series of rectangular pulses of the form

$$\frac{f(t_0) + f(t_1)}{2} t_0 < t < t_1; \frac{f(t_1) + f(t_2)}{2} t_1 < t < t_2; \text{ etc.}$$

Then:

$$g(\omega) = \frac{1}{2\pi} \left[\int_{t_0}^{t_1} \frac{f(t_0) + f(t_1)}{2} e^{-i\omega t} dt + \int_{t_1}^{t_2} \frac{f(t_1) + f(t_2)}{2} e^{-i\omega t} dt \right. \\ \left. + \dots + \int_{t_i}^{t_{i+1}} \frac{f(t_i) + f(t_{i+1})}{2} e^{-i\omega t} dt + \dots \right] .$$

Integrating gives:

$$g(\omega) = \frac{1}{2\pi} \left[\frac{f(t_0) + f(t_1)}{-2i\omega} (e^{-i\omega t_1} - e^{-i\omega t_0}) \right.$$

$$\begin{aligned}
& + \frac{f(t_1) + f(t_2)}{-2i\omega} (e^{-i\omega t_2} - e^{-i\omega t_1}) + \dots \\
& + \frac{f(t_i) + f(t_{i+1})}{-2i\omega} (e^{-i\omega t_{i+1}} - e^{-i\omega t_i}) + \dots \Big].
\end{aligned}$$

and,

$$\begin{aligned}
g(\omega) = & \frac{-1}{4\pi i\omega} \left[-e^{-i\omega t_0} (f(t_0) + f(t_1)) \right. \\
& + \sum_{i=1}^{n-1} (f(t_{i-1}) - f(t_{i+1})) e^{-i\omega t_i} \\
& \left. + e^{-i\omega t_n} (f(t_{n-1}) + f(t_n)) \right].
\end{aligned}$$

Substituting $\exp(-i\theta) = \cos\theta - i\sin\theta$ yields:

$$\begin{aligned}
g(\omega) = & \frac{-1}{4\pi i\omega} \left[(f(t_{n-1}) + f(t_n)) (\cos\omega t_n - i\sin\omega t_n) \right. \\
& - (f(t_0) + f(t_1)) (\cos\omega t_0 - i\sin\omega t_0) \\
& \left. + \sum_{i=1}^{n-1} (f(t_{i-1}) - f(t_{i+1})) (\cos\omega t_i - i\sin\omega t_i) \right].
\end{aligned}$$

Thus the Real part of $g(\omega)$, $\text{Re}[g(\omega)]$, and the Imaginary, $\text{Im}[g(\omega)]$,

are:

$$\begin{aligned} \text{Re}[g(\omega)] = \frac{1}{4\pi\omega} & \left[\sum_{i=1}^{n-1} [(f(t_{i-1}) - f(t_{i+1})) \sin \omega t_i] \right. \\ & - (f(t_0) + f(t_1)) \sin \omega t_0 \\ & \left. + (f(t_{n-1}) + f(t_n)) \sin \omega t_n \right]. \end{aligned}$$

$$\begin{aligned} \text{Im}[g(\omega)] = \frac{1}{4\pi\omega} & \left[\sum_{i=1}^{n-1} [(f(t_{i-1}) - f(t_{i+1})) \cos \omega t_i] \right. \\ & - (f(t_0) + f(t_1)) \cos \omega t_0 \\ & \left. + (f(t_{n-1}) + f(t_n)) \cos \omega t_n \right]. \end{aligned}$$

APPENDIX III

Derivation of the Fourier Inverse Transform for Digitized Pulses

Given two curves $A(\omega)$ and $B(\omega)$ such that:

$$A(\omega) = \frac{1}{2\pi} \int_{-\infty}^{\infty} f(t) \cos \omega t dt$$

$$B(\omega) = \frac{i}{2\pi} \int_{-\infty}^{\infty} f(t) \sin \omega t dt.$$

Then an original function can be assumed (9, p. 523) such that:

$$f(t) = f_1(t) + f_2(t)$$

$$= \int_{-\infty}^{\infty} A(\omega) \cos \omega t d\omega - i \int_{-\infty}^{\infty} B(\omega) \sin \omega t d\omega$$

Consider the digitized curves $A(\omega)$ and $B(\omega)$ such that:

$$A(\omega) = \begin{cases} \frac{A(0) + A(\omega_1)}{2} & 0 < \omega < \omega_1 \\ \frac{A(\omega_1) + A(\omega_2)}{2} & \omega_1 < \omega < \omega_2 \quad \text{etc.}, \end{cases}$$

and similarly for $B(\omega)$.

Consider $f_1(t)$ defined over a finite set of frequencies and

written in the form:

$$f_1(t) = 2 \left[\int_0^{\omega_1} \frac{A(0) + A(\omega_1)}{2} \cos \omega t d\omega + \int_{\omega_1}^{\omega_2} \frac{A(\omega_1) + A(\omega_2)}{2} \cos \omega t d\omega + \dots \right]$$

Integration yields:

$$f_1(t) = \frac{2}{t} \left[\frac{A(0) + A(\omega_1)}{2} (\sin \omega_1 t + 0) \right. \\ \left. + \frac{A(\omega_2) + A(\omega_1)}{2} (\sin \omega_2 t - \sin \omega_1 t) + \dots \right].$$

Similarly for B(ω),

$$f_2(t) = \frac{-2}{t} \left[\frac{B(0) + B(\omega_1)}{2} (\cos \omega_1 t - 1) \right. \\ \left. + \frac{B(\omega_1) + B(\omega_2)}{2} (\cos \omega_2 t - \cos \omega_1 t) + \dots \right].$$

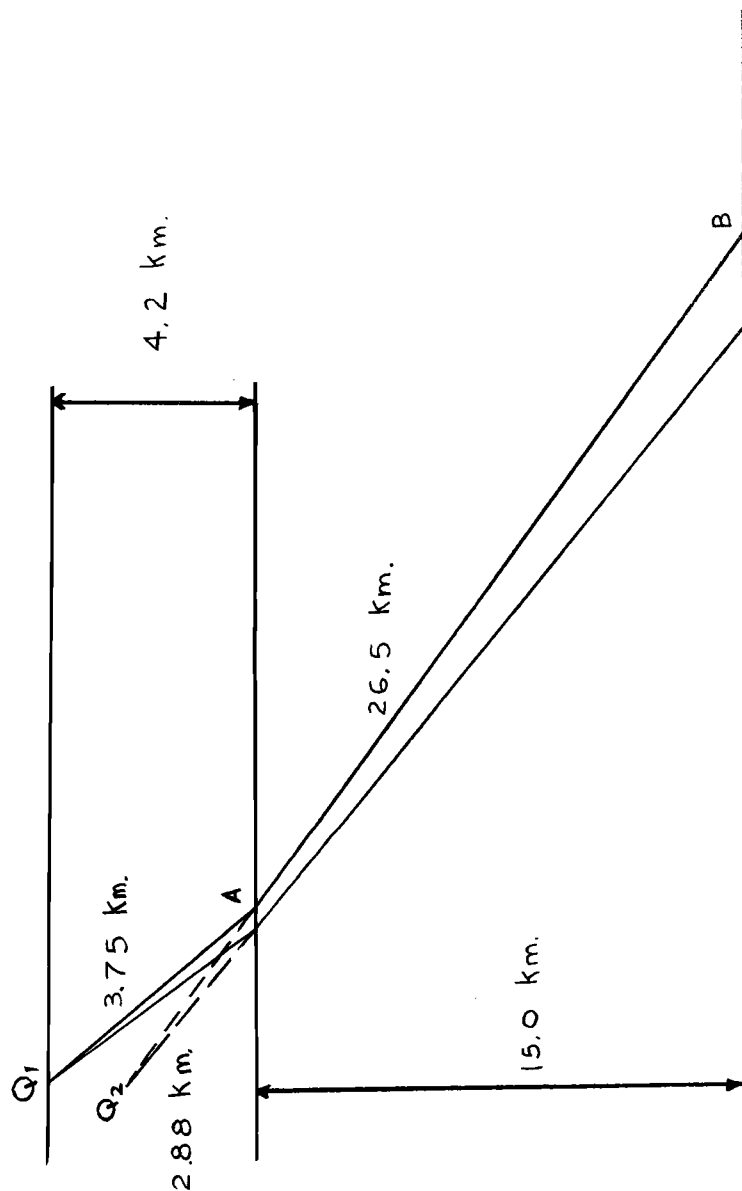
If the spectrum is digitized from $\omega = 0$ to $\omega = \omega_n$ the summations can be expressed as follows:

$$f_1(t) = \frac{-2}{t} \left[\sum_{i=1}^{n-1} \left[\frac{A(\omega_{i+1}) - A(\omega_{i-1})}{2} \sin \omega_i t \right] \right. \\ \left. - \frac{A(\omega_n) + A(\omega_{n-1})}{2} \sin \omega_n t \right]$$

$$f_2(t) = \frac{-2}{t} \left[\sum_{i=1}^{n-1} \frac{B(\omega_{i-1}) - B(\omega_{i+1})}{2} \cos \omega_i t + \frac{B(0) + B(\omega_1)}{2} \right. \\ \left. + \frac{B(\omega_{n-1}) + B(\omega_n)}{2} \cos \omega_n t \right].$$

APPENDIX IV

Virtual Source (18, p. 1593-1594)



What has been done graphically in the following figure is to construct a source for a two layered model which gives the same energy and amplitude at the point of critical refraction as the original source in a five layered case.

As an example of the method used, consider sources Q_1 and Q_2 .

Q_1 is the original source and Q_2 is a source in which the first layer has been replaced by the same media as layer two.

At point B, Q_1 and Q_2 would be indistinguishable if at point A they had the same energy and amplitude over the small increment of subtended angle. This would be satisfied when (18, p. 1594);

$$\frac{Q_1}{3.75} = \frac{Q_2}{2.88} .$$

This gives Q_2 in terms of Q_1 and effectively removes the first layer.

This process is repeated until only two layers remain and the resultant source, Q_4 , is in terms of Q_1 the original source. For this model model $Q_4 = 0.24 Q_1$.